IRAQI JOURNAL OF APPLIED PHYSICS LETTERS

Iraqi Journal of Applied Physics Letters (IJAPLett) is a scientific periodical sponsored and published by the Iraqi Society for Alternative and Renewable Energy Sources and Techniques (I.S.A.R.E.S.T.).

The Editorial Board is responsible for the scientific content and other editorial matters relating to the Journal. Manuscripts submitted are first screened by the editors; those on subject matters within the scope of the IJAPLett are sent to an expert referee for evaluation and may be sent to a second reviewer if necessary. This screening process helps to assure an appropriate focus as well as high scientific quality of the Journal. The IJAPLett welcomes submission of papers and letters in applied physics and related fields of science, engineering and technology. They should have something in common with what we now publish on inanimate materials and processes therein: structures, transport, physical, electrical, dielectric, magnetic, and optical properties. Our basic criterion stated below will continue to apply: papers must contain science, especially physics, and there must be an application. We advise authors submitting papers to suggest the names of at least two possible reviewers, with full information on addresses, phone and email. Suggestions of reviewers are welcome regardless of the subject.

SPONSORED AND PUBLISHED BY

THE IRAQI SOCIETY FOR ALTERNATIVE AND RENEWABLE ENERGY SOURCES AND TECHNIQUES (I.S.A.R.E.S.T.)

PRINTED IN IRAQ **ISSN 1999-656X**

" INSTRUCTIONS TO AUTHORS "

CONTRIBUTIONS

Contributions to be published in this journal should be original research works, i.e., those not already published or submitted for publication elsewhere, individual papers or letters to editor.

SUBMISSION OF MANUSCRIPTS

Manuscripts should be submitted to the editor at the mailing address:

Iraqi Journal of Applied Physics Letters
Editorial Board
P. O. Box 55259, Baghdad 12001, IRAQ
ijaplett@ijap.org , editor@ijap.org

MANUSCRIPTS

Two hard copies with soft copy on a compact disc (CD) should be submitted to Editor in the following configuration:

- Double-spaced one-side A4 size with 2.5 cm margins of all sides
- Times New Roman font (16pt bold for title, 14pt bold for names, 12pt bold for headings, 12pt regular for text)
- Letters should not exceed 10 pages.
- Manuscripts presented in English only are accepted.
- English abstract not exceed 150 words
- 4 keywords (at least) should be maintained on (PACS preferred)
- Author(s) should express all quantities in SI units
- Equations should be written in equation form (*italic* and symbolic)
- Figures and Tables should be separated from text
- Figures and diagrams can be submitted in colors for assessment and they will be returned to authors after provide printable copies
- Charts should be indicated by the software used for
- Only original or high-resolution scanner photos are accepted
- For electronic submission, articles should be formatted with MS-Word software.

AUTHOR NAMES AND AFFILIATIONS

It is IJAPLett policy that all those who have participated significantly in the technical aspects of a paper be recognized as co-authors or cited in the acknowledgments. In the case of a paper with more than one author, correspondence concerning the paper will be sent to the first author unless staff is advised otherwise.
Author name should consist of first name, middle initial, last name. The author affiliation should consist of the following, as applicable, in the order noted:
- Company or college (with department name or company division)
- Postal address
- City, state, zip code, country
- Telephone, and e-mail

REFERENCES

The references should be brought at the end of the article, and numbered in the order of their appearance in the paper. The reference list should be cited in accordance with the following examples:

[1] X. Ning and M.R. Lovell, "On the Sliding Friction Characteristics of Unidirectional Continuous FRP Composites", *ASME J. Tribol.*, 124(1) (2002) 5-13.
[2] M. Barnes, "Stresses in Solenoids", *J. Appl. Phys.*, 48(5) (2001) 2000–2008.
[3] J. Jones, "Contact Mechanics", Cambridge University Press (Cambridge, UK) (2000), Ch.6, p.56.
[4] Y. Lee, S.A. Korpela and R. Horne, "Structure of Multi-Cellular Natural Convection in a Tall Vertical Annulus", Proc. 7th International Heat Transfer Conference, U. Grigul et al., eds., Hemisphere (Washington DC), 2 (1982) 221–226.
[5] M. Hashish, "Waterjet Technology Development", High Pressure Technology, PVP-Vol. 406 (2000), 135-140.
[6] D.W. Watson, "Thermodynamic Analysis", ASME Paper No. 97-GT-288 (1997).
[7] C.Y. Tung, "Evaporative Heat Transfer in the Contact Line of a Mixture", Ph.D. thesis, Rensselaer Polytechnic Institute, Troy, NY (1982).

PROOFS

Authors will receive proofs of papers and are requested to return one corrected hard copy with a WORD copy on a compact disc (CD). New materials inserted in the original text without Editor permission may cause rejection of paper.

COPYRIGHT FORM

Author(s) will be asked to transfer copyrights of the article to the Journal soon after acceptance of it. This will ensure the widest possible dissemination of information.

OFFPRINTS

Authors will receive offprints free of charge and any additional offprints can be ordered.

SUBSCRIPTION AND ORDERS

Annual fees (4 issues per year) of subscription are:

- 50 US$ for individuals inside Iraq.
- 100 US$ for establishments inside Iraq.
- 100 US$ for individuals abroad.
- 200 US$ for establishments abroad.

Fees are reduced by 25% for I.S.A.R.E.S.T. members. Orders of issues can be submitted by contacting the editor-in-chief or editorial office at **subscription@ijap.org** to maintain the address of issue delivery and payment way.

The Use of Laser, Nanotechnology To Rapidly Detect Viruses

Waiting a day or more to get lab results back from the doctor's office soon could become a thing of a past. Using nanotechnology, a team of University of Georgia researchers has developed a diagnostic test that can detect viruses as diverse as influenza, HIV and RSV in 60 seconds or less. In addition to saving time, the technique could save lives by rapidly detecting a naturally occurring disease outbreak or bioterrorism attack. "It saves days to weeks," said lead author Ralph Tripp, Georgia Research Alliance Eminent Scholar in Vaccine Development at the UGA College of Veterinary Medicine. "You could actually apply it to a person walking off a plane and know if they're infected." **The technique, called surface enhanced Raman spectroscopy (SERS)**, works by measuring the change in frequency of a near-infrared laser as it scatters off viral DNA or RNA. This phenomenon is well known, but failed because the signal produced is inherently weak. The research group experimented several different metals and methods and found that placing rows of silver nanorods 10,000 times finer than the width of a human hair on the glass slides that hold the sample could enhance the signal. They found that the signal is best amplified when the nanorods are arranged at an 86-degree angle.

The technique is so powerful that it has the potential to detect a single virus particle and can also discern virus subtypes and those with mutations such as gene insertions and deletions. This specificity makes it valuable as a diagnostic tool, but also as a means for epidemiologists to track where viruses originate from and how they change as they move through populations. The researchers have shown that the technique works with viruses isolated from infected cells grown in a lab, and the next step is to study its use in biological samples such as blood, feces or nasal swabs. Preliminary results are so promising that it could be possible to create an online encyclopedia of Raman shift values. With that information, a technician could readily reference a Raman shift for a particular virus to identify an unknown virus.

Presently, viruses are first diagnosed with methods that detect the antibodies a person produces in response to an infection. These tests are prone to false positives because a person can still have antibodies in their system from a related infection decades ago. The tests are also prone to false negatives because some people don't produce high levels of antibodies. Because of these limitations, antibody based tests often must be confirmed with a test known as polymerase chain reaction (PCR), which detects the virus itself by copying it many times. The test can take anywhere from several days to two weeks, a too long period, especially in light of emerging threats such as H5N1 avian influenza.

LASER FLUORESCENCE could find life on MARS

edited by
Oday A. Hamadi
oday@ijap.org

A team of scientists from the United States and the UCL Mullard Space Science Laboratory has developed a technique using ultraviolet light to identify organic matter in soils that they say could be used to document the existence of life on Mars. The researchers' proposed instrumentation could operate on any Mars lander or rover, such as the current Phoenix mission or NASA's Mars Science Laboratory scheduled for launch in 2009 – both of which are looking at habitability – or the European Space Agency's ExoMars mission in 2013 that will look directly at the past or present existence of life on the red planet.

Chemical compounds called polycyclic aromatic hydrocarbons, or PAHs, often are found on comets, meteorites and in space between the stars, and are considered candidates for being one of the earliest forms of organic matter in the universe. Like living organisms, these molecules fluoresce when excited by ultraviolet light, making them an ideal target for using this new technology, according to Martin Fisk, a professor of marine geology at Oregon State University and a co-author of the study.

"Since PAHs are found on meteorites, we would expect some of that material to fall from space onto the surface of Mars," Fisk said. *"But we also know the surface is bombarded by ultraviolet light and cosmic rays, which would destroy organic matter. Computer simulations, including those carried out (by co-authors at) University College London, suggest that the organic material is protected under the surface of Mars, down below a meter or so, and can be brought up via a drill and identified."*

Michael Storrie-Lombardi, lead author and Director of the Kinohi Institute in Pasadena says: *"The techniques we are using have been employed every day in the safety of our laboratories for almost a hundred years. Recently the technology has become available to perfrom these experiments during remote surveys of other planets."*

In their experiment, the scientists created a fine, dusty soil by crushing a peridotite rock from a nickel mine in Riddle, Ore., that they say closely replicates the Martian surface material. A meteorite found in France, originating from Mars, consisted of 88 percent olivine, while the Oregon peridotite was 90 percent olivine.

They infused the peridotite granules with PAHs at a level of 50 parts per million, which is what they would expect to find on a meteorite, then took about a tablespoon of the soil and exposed it to different light waves from a meter away.

Using colored filters from the panoramic camera, or PanCam, that was the backup instrument for the Beagle 2-Lander, they were able to clearly identify as little as 1.5 micrograms of the organic material and pinpoint different PAHs by variations in their fluorescent response. The Beagle 2 made it to Mars in 2003, but was lost on approach and assumed to have crashed onto the Martian surface.

Two of the study's scientists – Storrie-Lombardi and Professor Jan-Peter Muller, of the UCL MSSL – carried out the optic experiments in the laboratory and at Silver Lake, California, a well-known Mars analog study site. As part of their tests, they set up a rig that could work under different conditions not dissimilar from the final system that would be mounted on a Mars lander or rover.

"Being able to test the fluorescence signature both under laboratory conditions and

in the field has been critical to being confident that such a system will work on the surface of Mars," said Muller.

Professor Andrew Coates also of the UCL MSSL, a co-author of the study and principal investigator of the international ExoMars PanCam team, said the challenge is to make the instrument light enough to be flown, and robust enough to survive the cold, minus-120 degree (C) Martian nights.

"With ExoMars PanCam, we already have thrilling science – stereo and zoom imagery giving the context for all the ExoMars life detection experiments and the use of colored filters to provide rock identification and atmospheric composition," Coates said. *"If the team can show this is light and rugged enough, we will propose taking it to Mars."*

Proving such durability will be a challenge, according to Andrew Griffiths, a co-author on the paper and the instrument manager for the ExoMars PanCam team. *"Getting to Mars is tough, as we found with Beagle 2,"* he pointed out. *"Surviving the surface conditions is even tougher, particularly with new technology."*

While using fluorescence to illuminate organic material has been done for decades, light sources were too large and unwieldy to use for a robotic mission to another planet, said Storrie-Lombardi. However, new generations of light-emitting diodes, or LEDs, are very small, reliable and energy efficient, he added.

"Placed on a Mars rover, one of these LEDs positioned a few centimeters from a target can easily provide enough light to produce fluorescence in small polycyclic aromatic hydrocarbons," Storrie-Lombardi said. *"But even more encouraging is the very recent development of a small 375 nanometer laser diode that can illuminate anything a PanCam can see, including geological layers and crevices high up on an otherwise inaccessible rock outcrop."*

Professor Muller added: *"This laser is now undergoing rigorous tests in the laboratory under Mars-like conditions prior to showing that it is flight-ready, even at this late stage, to be seriously considered to be launched in only five years' time."*

The instrument appears to be ***"an ideal initial survey tool,"*** Storrie-Lombardi pointed out. *"It requires no sample preparation, does not destroy sample material and requires only electrical power to operate, conserving precious water and other consumable resources for sister instruments."*

Since the Viking mission to Mars 30 years ago, no mission to Mars has focused exclusively on searching for evidence of organic material or biological activity, Storrie-Lombardi said. Now the ongoing Phoenix mission and the planned Mars Science Laboratory and ExoMars missions are positioned to reverse that trend.

"The addition of an ultraviolet triage system to search for hints of organic material fits well into the extensive suite of organic detection instruments planned for the MSL and ExoMars expedition," he said.

Oregon State's Fisk, whose research has focused in part on the study of microbes that grow in inhospitable locations, said the best chance of finding organic material on Mars would be wherever there is, or was, water – locations where rocks have experienced weathering.

"These are energy-rich environments for microbial life," said Fisk, a professor in OSU's College of Oceanic and Atmospheric Sciences.

Fisk and his colleagues have spent much of the past dozen years studying microbes that can break down igneous rock and live in the obsidian-like volcanic glass. They first identified the bacteria through their signature tunnels then were able to extract DNA from the rock samples – which have been found in such diverse environments on Earth as below the ocean floor, in deserts and on dry mountaintops.

Fisk and Storrie-Lombardi – along with other scientists at OSU and the Jet Propulsion Laboratory – previously collaborated on a study that found bacteria 4,000 feet below the ocean surface in Hawaii that they reached by drilling through the solid volcanic rock base of Mauna Kea.

* * *

Commercial Applications of NANOTECHNOLOGY in Medicine and Health

Professor Stephen Wood
Professor Richard Jones
Alison Geldart

Background
The medical area of nanoscience application is one of the most potentially valuable, with many projected benefits to humanity. Cells themselves are very complex and efficient nano-machines, and chemists and biochemists have been working at the nanoscale for some time without using the nano label. Some areas of nanoscience aim to learn from biological nanosystems, while others are focusing on the integration of the organic and inorganic at the nanoscale. Many possible applications arising from this science are being researched.

Implants and Prosthetics
The first field is implants and prosthetics. With the advent of new materials, and the synergy of nanotechnologies and biotechnologies, it could be possible to create artificial organs and implants that are more akin to the original, through cell growth on artificial scaffolds or biosynthetic coatings that increase biocompatibility and reduce rejection. These could include retinal, cochlear and neural implants, repair of damaged nerve cells, and replacements of damaged skin, tissue or bone.

Diagnostics Using Sensors and Micro Electro Mechanical Systems (MEMS)
The second area is diagnostics. Within MEMS (Micro Electro Mechanical Systems), laboratory-on-a-chip technology for quicker diagnosis which requires less of the sample is being developed in conjunction with microfluidics. In the medium term, it could be expected that general personal health monitors may be available. Developments in both genomics and nanotechnology are likely to enable sensors that can determine genetic make-up quickly and precisely, enhancing knowledge of people's predisposition to genetic-related diseases.

Drug Delivery Using Nanoparticles and Molecular Carriers
Finally, drug delivery is likely to benefit from the development of nanotechnology. With nanoparticles it is possible that drugs may be given better solubility, leading to better absorption. Also, drugs may be contained within a molecular carrier, either to protect them from stomach acids or to control the release of the drug to a specific targeted area, reducing the likelihood of side effects. Such drugs are already beginning pre-clinical or clinical trials, adhering to the strict regulatory requirements for new pharmaceuticals. Due to this, development costs are often high and outcomes of research sometimes limited.

Lab on a Chip and Advanced Drug Delivery Systems
The ultimate combination of the laboratory-on-a-chip and advanced drug delivery technologies would be a device that was implantable in the body, which would continuously monitor the level of various biochemicals in the bloodstream and in response would release appropriate drugs. For example, an insulin-dependent diabetic could use such a device to continuously monitor and adjust insulin levels autonomously. There is no doubt that this is the direction that current advances in which microfluidics and drug delivery are heading.

Rana O. Mahdi
Ban A.M. Bader
Haithem S. Dawood
Aseel A.K. Hadi

School of Applied Sciences, University of Technology, Baghdad, Iraq

Effect of Chirping on Received Pulse Shape in Optical Fiber Communications

In this work, the effect of chirping on the pulse broadening and wavelength shift in the optical fiber communications was studied. A numerical analysis based on tracing the pulse propagating through an optical fiber was presented to determine the role of chirping in pulse broadening. Consequently, the wavelength shift resulted from the chirping effect was deduced analytically.

Keywords: Chirping, Pulse shape, Wavelength spectrum, Optical communications
Received: 10 February 2009, **Revised**: 27 April 2009, **Accepted**: 8 May 2009

1. Introduction

Short-pulse high-repetition-rate lasers are key elements for future high-speed optical communications systems and all-optical logic circuits. Actively mode-locked lasers are promising candidates, especially when synchronization between optical and electrical signals is required [1-4]. Pulse compression is an established technique for generating optical pulses shorter than those produced by lasers or amplifiers. Compressors based on single-mode fibers are limited to nanojoule pulse energies by higher-order nonlinear effects and ultimately by damage to the fiber. Thus, new approaches are needed for compression of the high-energy pulses that are now available from chirped-pulse amplifiers [5].

One very important feature of ultrashort laser pulses is the close relation between the pulse duration (τ) and the spectral bandwidth ($\Delta\omega$), which is manifested in the time-bandwidth product as:

$$\tau\Delta\omega \geq 2\pi c_B \qquad (1)$$

where c_B is a constant that depends on the shape of the pulse and ω is the angular frequency related to the frequency (f) and wavelength (λ) through:

$$\omega = 2\pi f = \frac{2\pi c}{\lambda} \qquad (2)$$

It follows directly from Eq. (1) that the minimum achievable duration is limited by the spectrum of the pulse. In other words, in order to produce ultrashort pulses, a very broad spectral bandwidth is needed. The shortest possible pulse, for a given spectrum, is known as the "transform-limited pulse duration". It should be noted that Eq. (1) is not equality, i.e., the product can very well exceed ($2\pi c_B$). if the product exceeds ($2\pi c_B$), the pulse is no longer transform-limited and all frequency components that constitute the pulse do not coincide in time, i.e., the pulse exhibits frequency modulation. This frequency modulation is very often referred to as a ***chirp*** since birdsong also changes frequency as a function of time. The bandwidth of a Gaussian pulse with a chirp can be said to constitute two parts, the first part is the bandwidth needed to support the duration of the stretched pulse (i.e. smaller than if the pulse had no chirp), and a second part needed to support the frequency variation across the pulse [6-9].

For laser diodes under direct modulation, the photocurrent pulse is more complex when the chirping effect is considered. The chirping effect is caused by refractive index modulation of the laser cavity. As a result, the output spectrum $g_S(\lambda\text{-}\lambda_c)$ is time varying. For single-mode laser diodes, the range of wavelength shifts during turn-on and turn-off transitions can be much larger than that at the steady state linewidth. In case of laser pulse propagating through an optical fiber, the chirping effect may originate from the refractive index modulation of the fiber material considered as an optical medium [10].

2. Analysis

For simple consideration, assume the slope of the spectrum is time invariant. Although this assumption may not be valid under large modulation, a time-varying spectrum shape is difficult to model and strongly depends on individual devices used [11]. Therefore, only the case of time-invariant spectrum shape is considered here. With this assumption, the time-varying spectrum can be modelled as

$$g_S = g_S[\lambda - \lambda_0 - \Delta\lambda_c(t)] \qquad (3)$$

where $\Delta\lambda_c(t)$ is the wavelength shift from the central wavelength λ_0 due to chirping. When a laser is turned on, the wavelength shift is negative and called **"blue shift"**. When the laser is turned off, the wavelength is positive and called **"red shift"** [12]. Because the wavelength shift is proportional to the shift of the refractive index from its steady state value during modulation, we can have

$$\Delta\lambda_c(t) = \begin{cases} 0 & if \quad t < t_d \\ -\beta_{chirp}\Delta\lambda \sin(\omega_r[t-t_d])e^{-\alpha(t-t_d)} & if \quad t_d < t < T_0 \\ -\beta_{chirp}\Delta\lambda \sin(\omega_r[T_0-t_d])e^{-\alpha(T_0-t_d)}e^{-\alpha_{off}(t-T_0)} + \beta_{chirp}\Delta\lambda(1-e^{-\alpha_{off}(t-T_0)}) & if \quad T_0 < t \end{cases} \tag{4}$$

where β_{chirp} is the ratio of the peak wavelength shift due to chirping to the linewidth at the steady state. Given this wavelength shift, the pulse output at the other end of the fiber is

$$p(t) = \int \frac{1}{D_{\text{int}}L} g_S\left(\frac{t - t_{g0} - t' - D_{\text{int}}L\Delta\lambda_c(t')}{D_{\text{int}}L}\right) p_S(t')dt' \tag{5}$$

where $p_S(t)$ is the pulse input to the fiber. Therefore, the fiber transfer function can be modified as

$$h_{fiber}(t) = \frac{1}{D_{\text{int}}L} g_S\left(\frac{t + t_{g0} + D_{\text{int}}L\Delta\lambda_c(t)}{D_{\text{int}}L}\right) \tag{6}$$

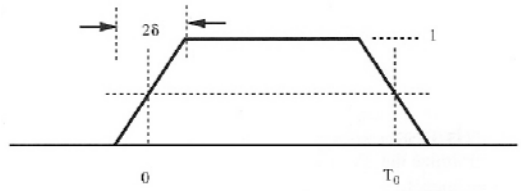

Fig. (1) The finite slope pulse considered in the modelling

Although the chirping effect can be computed numerically using Eq. (5), it is instructive to use a simplified model to gain insight into the effect. The model first assumes an output pulse from a laser diode of a form similar to the finite slope pulse shown in Fig. (1). That is, it assumes

$$p_S(t) = \begin{cases} \frac{t}{\delta_c} & if \quad 0 < t < \delta_c \\ 1 & if \quad \delta_c < t < T_0 \\ 1 - \frac{t - T_0}{\delta_c} & if \quad T_0 < t < T_0 + \delta_c \\ 0 & if \quad otherwise \end{cases} \tag{7}$$

The first portion δ_c of the pulse is assumed to b the portion where the central wavelength linearly increases from λ_0-$\beta_{chirp}\Delta\lambda$ to the steady state value (λ_0). The tail portion δ_c of the pulse is assumed to b the portion where the central output wavelength linearly increases from the steady state value (λ_0) to $\lambda_0+\beta_{chirp}\Delta\lambda$. In the middle portion, the pulse is assumed to have a constant central wavelength λ_c.

Let $p_1(t)$ be the beginning portion of the pulse that has chirping with output wavelength linearly decreasing to the steady state. For $0<t<\delta_c$, the propagation delay over distance L is

$$t_g(t) = t_{g0} + \frac{t - \delta_c}{\delta_c} D_{\text{int}}\beta_{chirp}\Delta\lambda L \tag{8}$$

where t_{g0} is the propagation delay at the steady state wavelength. If $p_1(t)$ is partitioned into many small intervals,

$$p_1(t) = \lim_{\Delta t \to 0} \sum_i \frac{rect(t - t_i, \Delta t)}{\Delta t} p_1(t_i)\Delta t \tag{9}$$

where $t_i = i\Delta t$. The pulse after a distance L is

$$p_1(t,L) = \lim_{\Delta t \to 0} \sum_i \frac{rect(t - t_i - t_{g0} - \tau_c[t_i - \delta_c]/\delta_c, \Delta t)}{\Delta t} p_1(t_i)\Delta t \tag{10}$$

where $\tau_c = \beta_{chirp} D_{\text{int}} L\Delta\lambda$

By taking the limit $\Delta t \to 0$, one obtains

$$p_{1,out}(t) = \int \delta[t - t'(1+\tau_c/\delta_c) - t_{g0} + \tau_c] p_1(t')dt' = \frac{\delta_c}{\delta_c + \tau_c} p\left(\frac{t - t_{g0} + \tau_c}{1 + \tau_c/\delta_c}\right) \tag{11}$$

Similarly, for the tail portion of the pulse, which has chirping during the turn-off transition from T_0 to $T_0+\delta_c$, the output over distance L is

$$p_2(t,L) = \lim_{\Delta t \to 0} \sum_i \frac{rect(t - t_i - \tau_c(t_i/\delta_c) - T_0 - t_{g0}, \Delta t)}{\Delta t} p_2(t_i + T_0) \tag{12}$$

and

$$p_{2,out}(t,L) = \int \delta[t - T_0 - t_{g0} - t_i(1+\tau_c/\delta_c)] p_2(t'+T_0)dt' = \frac{\delta_c}{\delta_c + \tau_c} p_2\left(\frac{t - T_0}{1 + \tau_c/\delta_c}\right) \tag{13}$$

3. Results and Discussion

To obtain results of the modelling, both MATLAB-7.0 and SIMULATICS-3 software were employed. The output pulse over distance L according to this simplified model is illustrated in Fig. (2).

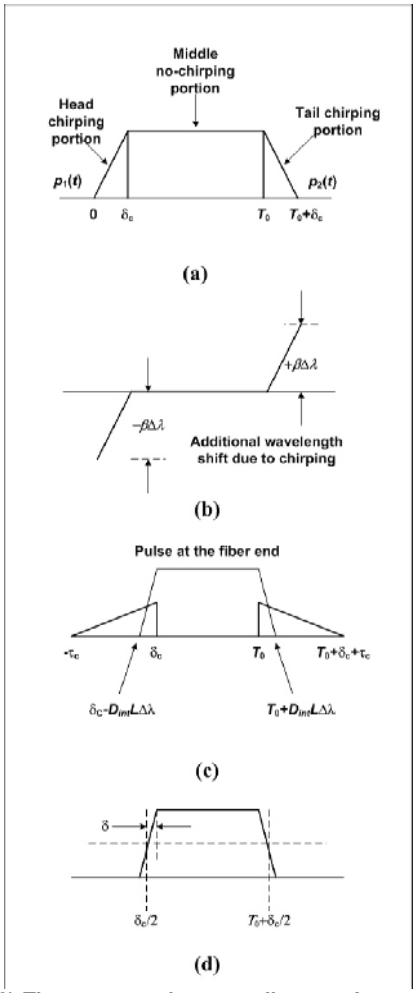

Fig. (2) The output pulse over distance *L* according to the simplified model. (a) the original pulse, (b) the chirping in the head and tail portions, (c) the pulse at the fiber end with fiber dispersion, (d) the approximation of the pulse shown in (c)

Figure (2a) shows the original pulse, which consists of three portions: the head, middle, and tail. The head and tail portions have chirping as shown in Fig. (2b). With fiber dispersion, the pulse at the fiber end is illustrated in Fig. (2c). Here the effect of fiber dispersion on the middle portion of the pulse is also considered [3,13]. To quantify the chirping effect together with the fiber dispersion effect on pulse broadening, one can approximate the pulse shown in Fig. (2c) as the pulse in Fig. (2d). To find the corresponding pulse broadening factor (δ) in Fig. (1), equate the power of the head portion of the pulse between $-\tau_c$ and $\delta_c/2$ to the power of beginning portion of the pulse from $-\delta$ to 0 in Fig. (2).

If $D_{\text{int}}L\Delta\lambda=\tau_c/\beta_{chirp}<\delta_c/2$, the middle portion caused by fiber dispersion is still within $\delta_c/2$ and $T_0+\delta_c/2$. Therefore, its broadening is not important, and the pulse broadening is purely due to chirping. In this case, the equivalent pulse broadening parameter (δ) is

$$\frac{1}{4}\delta=\frac{1}{2}\delta_c\left(\frac{\tau_c+\delta_c/2}{\tau_c+\delta_c}\right)^2 \qquad (14)$$

If $D_{\text{int}}L\Delta\lambda>\delta_c/2$, the fiber dispersion for the middle portion should be included. In this case, the equivalent pulse broadening parameter (δ) is

$$\frac{1}{4}\delta=\frac{1}{2}\delta_c\left(\frac{\tau_c+\delta_c/2}{\tau_c+\delta_c}\right)^2+\frac{1}{2}\frac{(\tau_c/\beta_{chirp}-\delta_c/2)^2}{(\tau_c/\beta_{chirp})} \qquad (15)$$

The values of parameters included in Eq. (14) and (15) are tabulated in Table (1). Now, we have δ=0.364 ns at L=10km and δ=1.98 ns at L=100km.

Table (1) The values of parameters included in Eq. (14) and (15)

Parameter	Value
δ_c	0.2 s
$D_{int}\Delta\lambda$	10 ps/km
β_{chirp}	2
L	10 - 100 km
$D_{total}L$	1 ns
τ_c	2 ns

In order to explain the effect of dispersion limit due to chirping on the pulse broadening parameter (δ), three different values of the total fiber chirping dispersion (τ_c) (1, 2, 4) were considered to plot the relation between the pulse broadening parameter (δ) and chirping ratio (β_{chirp}) as shown in Fig. (3). We can observe that increasing value of (τ_c) caused corresponding increase in the pulse broadening parameter. However, the behaviour of this function is identical with some multiple term.

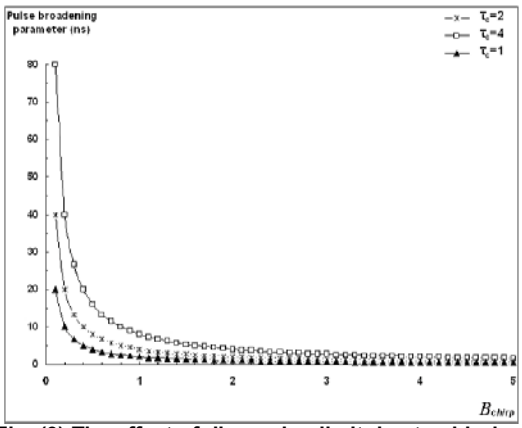

Fig. (3) The effect of dispersion limit due to chirping on the pulse broadening parameter (δ) for three different values of the total fiber chirping dispersion (τ_c) (1, 2, 4)

Similarly, three values of pulse partition (δ_c) (0.02, 0.2, 0.5) were considered to plot the same δ-β_{chirp} relation in Fig. (4) to explain the effect of pulse partition. It is clear that the function did not vary as the δ_c-value did, i.e., the pulse partition has no effect on the pulse broadening parameter. Hence, the bit rate, which is inversely proportional to the pulse broadening parameter (=1/8δ). So, the bit rate is not affected by the variation of pulse partition (δ_c) but extremely affected by the total fiber chirping dispersion (τ_c), as shown in Fig. (5).

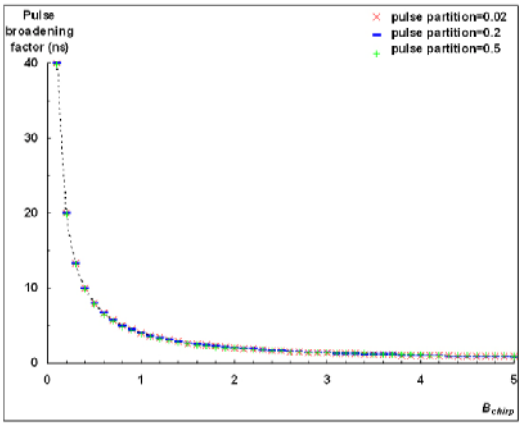

Fig. (4) The effect of dispersion limit due to chirping on the pulse broadening parameter (δ) for three values of pulse partition (δ_c) (0.02, 0.2, 0.5)

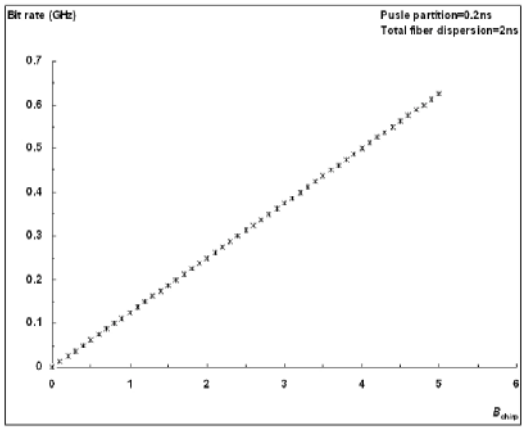

Fig. (5) Relation between bit rate (B) in GHz and chirping ratio (β_{chirp}) at pulse partition of (0.2ns) and total fiber dispersion of (2ns)

4. Conclusions

With respect to results obtained from this study, chirping has reasonable effect on the pulse broadening and wavelength shift of a laser pulse propagating through an optical fiber employed in optical communications. Wavelength shift due to fiber chirping dispersion is represented by two red and blue shifts. So, such shifts should be avoided by controlling chirping effect because they may cause reasonable distortion in the pulse spectrum exiting from the optical fiber. As well, pulse broadening is resulted from chirping dispersion effect and it should be controlled precisely in order not to exceed certain limits, which highly affect the bit rate of the transmitted data through the optical fiber communications system.

References

[1] K. L. Hall and K. A. Rauschenbach, *Opt. Lett.*, 23, 1998, 1271.
[2] T.J. Xia et al., *IEEE Photon. Technol. Lett.,* 10, 1998, 153.
[3] J. Jasapara and W. Rudolph, *Opt. Lett.*, 24(11), 1999, 777-779.
[4] L. Gallmann et al., *Opt. Lett.*, 24(18), 1999, 1314-1316.
[5] X. Liu, L. Qian and F. Wise, *Opt. Lett.*, 24(23), 1999, 1777-1779.
[6] Z. Cheng et al., *Opt. Lett.*, 24(4), 1999, 247-249.
[7] C. Dorrer et al., *Opt. Lett.*, 24(22), 1999, 1644-1646.
[8] T. Harimoto, M. Aoyama and K. Yamakawa, *Jpn. J. Appl. Phys.*, 41, 2002.
[9] A. Efimov, D. H. Reitze, *Opt. Lett.*, 23, 1998, 1612-1614.
[10] M.K. Liu, **"Principles and Applications of Optical Communications"**, McGraw-Hill Co. (Chicago), 1996, p.346.
[11] B. Haase, *Opt. Lett.*, 24(8), 1999, 543-545.
[12] J. Kunde et al., *Appl. Phys. Lett.*, 73(21), 1998, 3025-3027.
[13] F. Louradour et al., *Opt. Lett.*, 24(19), 1999, 1361-1363.

Performance Optimization of Multi-Quantum Wells Laser Used in Optical Communications

Sahra S. Jasim

School of Applied Sciences, University of Technology, Baghdad, Iraq

In this work, an analytical treatment of some design parameters of multi-quantum well semiconductor laser aiming to optimize the performance of such systems is presented. The treatment concentrates on three main parameters; the reflectivity of the front mirror, the effective lifetime of the photon inside laser cavity, and the number of quantum wells in the laser structure. These three parameters relate to several other parameters which impose to achieve design compensation. Such compensation can be simulated by analytical treatments because the characteristics of these lasers have been established well in form of small and large signal solutions. These lasers are increasingly studied due to their characteristic features in optical communications architectures, low-dimensioned photonics and optoelectronics devices.

***Keywords*:** MQW, Semiconductor laser, Optical communications, Optimization
Received: 30 March 2009, **Revised**: 25 April 2009, **Accepted**: 9 May 2009

1. Introduction

Semiconductor lasers are excellent optical sources for several applications including: high-speed optical time-division multiplexed (OTDM) communication systems, optical clocking and sampling, etc [1]. When a voltage is applied to a degenerated *pn* junction device, considerable electrons and holes are injected into the transition region. If the bias is large enough, the transition region contains a high concentration of conduction band electrons and a high concentration of valence band holes. In other words, a population inversion exists around the junction. This population inversion region is also called the active region.

Another condition to sustain continuous laser operation from the device is the optical cavity. Its main function is to implement a laser oscillator, or to build up the intensity of stimulated emissions by means of an optical resonator. Since only multiples of the half-wavelength can exist in an optical cavity, the radiation wavelength that can build up in the cavity is determined by the cavity length *L*,

$$L = M\frac{\lambda_0}{2n} \qquad (1)$$

where M is an integer, λ_0 is the free space wavelength, and n is the refractive index of the semiconductor. The resonant frequency of the cavity, i.e., a mode of cavity, satisfies the above relationship.

The device described thus far is a homo-junction laser, since both p and n regions are fabricated with the same semiconductor. The multiple quantum well structure schematically sketched in Fig. (1) extends the advantages of the single quantum well laser [1].

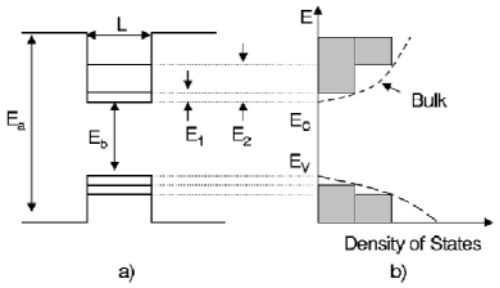

Fig. (1) (a) Schematic energy diagram of a semiconductor QW structure. E_a and E_b are the energy gaps that make up the barriers and well. E_1 and E_2 are the first two energy states confined in the well of width L. (b) Density of States in a quantum well and bulk material. The dashed curve represents the 3D density of states for bulk material while the solid line is the 2D density states for a particle confined to a quantum well [1]

The introduction of compressive strain into the multiple quantum well lasers leads to low internal loss, high quantum efficiency, low threshold current operation, and small line-width enhancement factors [2-4]. This configuration forms a rectangular quantum potential well from the energy bands. When the thickness of the narrow bandgap material, L, is on the order of the de Broglie wavelength of a thermalized electron ($\lambda=h/p$, where h is Planck's constant and p is the momentum of the electron), quantum size effects occur forming quantized energy states within the well [5]. These states represent the probability of having an electron or hole in

any respective position within the well and are found from the solution to the time independent Schrodinger wave equation in two dimensions.

2. The Model

Laser action and optical gain occur in a semiconductor because of the non-equilibrium of carriers that populate the bands. This state is attained as described above.

The absorption of incident photons is given by the absorption rate as

$$r_{abs} = P[1-f_n(E_2)]f_p(E_1)N_p(E) \quad (2)$$

While the stimulated emission rate is given as

$$r_{st} = Pf_n(E_2)[1-f_p(E_1)]N_p(E) \quad (3)$$

where P is the transition probability, N_p is the density of photons of energy E, and f_n and f_p are the Fermi functions. For lasing to occur, there must be more stimulated radiative processes than photon absorption processes, thus $r_{st}>r_{abs}$. This condition leads to $f_n(E_n)>f_p(E_p)$ where E_n-E_p is the transition energy from the conduction band to the valence band. This condition causes population inversion: where the concentration of electrons in the conduction band is greater than the concentration of holes in the valence band. The gain, represented by stimulated downward transitions of carriers, should be at least equal to the losses, stimulated upward transitions, for lasing to occur [2].

Longitudinal modes are formed along the length of the active region parallel to the semiconductor layers. These modes define laser resonance. This is the process whereby photons generated in the active region oscillate along the length perpendicular to the cleaved "mirror" facets producing gain and thus laser emission. The cavity is resonant because only certain frequencies (wavelengths) of light are allowed within it. These resonant frequencies are governed by the cavity length d. The appropriate choice will stimulate a certain wavelength while damping all others. This condition is

$$d = \frac{q\lambda}{2n} \qquad q = 1,2,3,... \quad (4)$$

where λ is the wavelength, and n is the effective index of refraction within the active region. The resonant frequency follows from this expression as

$$v_q = \frac{qc}{2nd} \qquad q = 1,2,3,... \quad (5)$$

where c is the speed of light. These frequencies are the longitudinal modes which are solutions to the Helmholtz equation with appropriate boundary conditions.

Rate equations for each longitudinal mode, λ, with photon density (S_λ) and carrier density (N_λ), which couple into this mode, are:

$$\frac{\partial N_\lambda}{\partial t} = \frac{J_\lambda}{q} - B_\lambda N_\lambda^2 - \frac{N_\lambda}{2\tau_0} + \sum_k \frac{N_\lambda}{\tau_{k,\lambda}} - \sum_k \frac{N_\lambda}{\tau_{k\lambda,\lambda}} - \frac{\partial S_\lambda}{\partial x}\frac{\partial x}{\partial t} \quad (6)$$

$$\frac{\partial S_\lambda}{\partial t} = \beta_\lambda B_\lambda N_\lambda^2 - \frac{S_\lambda}{\tau_{ph,\lambda}} + \frac{\partial S_\lambda}{\partial x}\frac{\partial x}{\partial t}, \qquad \lambda = 1,2,...,\lambda_{\max} \quad (7)$$

We will consider one mode with photon density (S), whose photon energy is closest to the peak gain, rather than using set of differentia; equations for all waveguide modes. The intensity of this mode will grow faster than all others and eventually dominate [8]. This simplification avoids the problem of finding the parameters and coefficients for every single mode. On the other hand, it does no enable to calculate the emission spectrum of the laser diode. For a single longitudinal mode, the rate equations reduce to:

$$\frac{\partial N}{\partial t} = \frac{J}{q} - BN^2 - \frac{N}{2\tau_0} - v_{gr}\Gamma l(N - N_{tr})S \quad (8)$$

$$\frac{\partial S}{\partial t} = \beta BN^2 - \frac{S}{\tau_{ph}} - v_{gr}\Gamma l(N - N_{tr})S \quad (9)$$

$$P_L = -v_{gr}SW\ln\frac{1}{\sqrt{R_1}} \quad (10)$$

Here, the photon lifetime (τ_{ph}) is related to the quality factor (Q) of the laser cavity as [6]:

$$\tau_{ph} = \frac{\lambda Q}{2\pi c} \quad (11)$$

Assuming a time harmonic solution and ignoring higher order terms, the rate equations become [7]

$$j\omega n_L = \frac{j_L}{q} - \frac{n_L}{\tau_{eff}} - v_{gr}\Gamma l(N-N_{tr})s_L - v_{gr}\Gamma n_L l S_0 \quad (12)$$

$$j\omega s_L = \frac{s_L}{\tau_{ph}} + v_{gr}\Gamma l(N-N_{tr})s_L + v_{gr}\Gamma n_L l S_0 \quad (13)$$

where τ_{eff} is the same as for LED. Using the following

$$\frac{1}{\tau_{ph}} = v_{gr}\Gamma l(N - N_{tr}) \quad (14)$$

These equations can be solved yielding

$$j_L = j\omega q n_L + qn_L\left(\frac{1}{\tau_{ph}} + v_{gr}\Gamma l S_0\right) + qn_L\frac{v_{gr}\Gamma l S_0}{j\omega\tau_{ph}} \quad (15)$$

Replacing n_1 by relating it to the small signal voltage v_1

$$v_L = \frac{mV_t n_L}{N_0} \quad (16)$$

The equation for the small signal current, i_1, can be written as

$$i_L = \left(j\omega C + \frac{1}{R} + \frac{1}{j\omega L}\right)v_L \quad (17)$$

where $C = \frac{qN_0A}{mV_t}$, A is the area of the laser diode and

$$m = \frac{N_0 e^{N/N_c}}{N_c(e^{N/N_c}-1)} + \frac{N_0 e^{N/N_v}}{N_v(e^{N/N_v}-1)} \quad (18)$$

$$\frac{1}{R} = C\left(\frac{1}{\tau_{eff}} + \Gamma l S_0 v_{gr}\right) \quad (19)$$

and

$$L = \frac{1}{C}\left(\frac{\tau_{ph}}{\Gamma l S_0 v_{gr}}\right) \quad (20)$$

Adding parasitic elements and the circuit described by the Eq. (16) we obtain the following equivalent circuit, where L_B is a series inductance, primarily due to the bond wire, R_S is the series resistance in the device and C_p is the parallel capacitance due to the laser contact and bonding pad [8].

The resistor R_d, in series with the inductor, L, is due to gain saturation [5] and can be obtained by adding a gain saturation term to Eq. (16). The optical output power is proportional to the current through inductor L, which is given by:

$$i_L = \frac{qAs}{\tau_{ph}} = qAsv_{gr}\left(\alpha + \frac{1}{L_C}\ln\frac{1}{\sqrt{R_1 + R_2}}\right) \quad (21)$$

and the corresponding power emitted from mirror R_1

$$P_L = sh\nu W v_{gr} \ln\frac{1}{\sqrt{R_1 + R_2}} \quad (22)$$

Ignoring the parasitic elements and the gain saturation resistance, R_d, we can find the AC responsivity P_L/i_L as:

$$\frac{P_L}{i_L} = \frac{h\nu}{q}\frac{\ln\frac{1}{\sqrt{R_1}}}{\ln\frac{1}{\sqrt{R_1 + R_2}} + \alpha L_C}\frac{1}{1 + j\omega\frac{L}{R} + (j\omega)^2 LC} \quad (23)$$

From which we find the relaxation frequency of the laser

$$\omega_0 = \frac{1}{\sqrt{LC}} = \sqrt{\frac{\Gamma S_0 l v_{gr}}{\tau_{ph}}} = \sqrt{\frac{\Gamma l P_0}{h\nu\tau_{ph} W \ln\frac{1}{\sqrt{R_1}}}} \quad (24)$$

or the relaxation frequency is proportional to the square root of the DC output power. The amplitude at the relaxation frequency relative to that at zero frequency equals [8]

$$\frac{P_L|_{\omega=\omega_0}}{P_L|_{\omega=0}} = \frac{R}{L\omega_0} = \frac{1}{\frac{1}{\omega_0\tau_{eff}} + \omega_0\tau_{ph}} \quad (25)$$

Comparing threshold currents of laser diodes with identical dimensions and material parameters but with a different number of quantum wells (m), we can find that the threshold currents are not simple multiples of that of a single quantum well laser.

Assuming that the modal gain (g) is linearly proportional to the carrier concentration in the wells and that the carriers are equally distributed between the m wells. For m quantum wells, the modal gain can be expressed as:

$$g = lm(N - N_{tr}) = lm\Delta N \quad (26)$$

where l is the differential gain coefficient and N_{tr} is the transparency carrier density.

Since the total modal gain is independent of the number of quantum wells, we can express the carrier density as a function of modal gain at lasing [6]:

$$N = \frac{g}{lm} + N_0 = \frac{\Delta N}{m} \quad (27)$$

Then the radiative recombination current at threshold is [8]

$$J_{th} = qB_1 m\left(N_{tr} + \frac{\Delta N}{m}\right)^2 = qB_1\left(N_{tr}^2 m + 2N_{tr}\Delta N + \frac{\Delta N^2}{m}\right) \quad (28)$$

where B_1 is the quantum-well radiative recombination rate coefficient

This means that the threshold current density is a constant plus a component which is proportional to the number of quantum wells. The last terms can be ignored for m>>1 and ΔN<<N_{tr}.

3. Results and Discussion

Figure (2) shows the variation of the quantum efficiency with the reflectivity of the front mirror of laser resonator at different cavity lengths (L). It is clear that the efficiency decreases with increasing reflectivity as well as increasing cavity length.

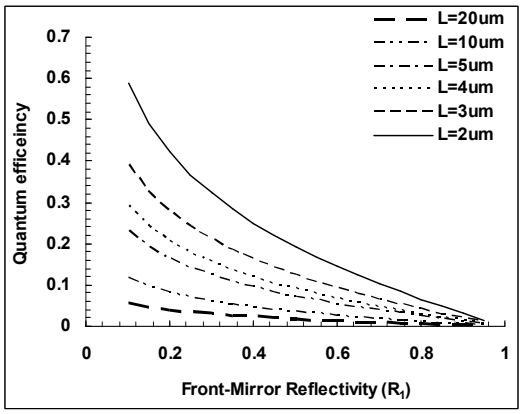

Fig. (2) Variation of quantum efficiency with the reflectivity of output mirror for different lengths of laser cavity (*L*)

Therefore, efficient lasers are obtained by reducing the waveguide losses, increasing the reflectivity of the back mirror, decreasing the reflectivity of the front mirror and decreasing the length of the cavity. Decreasing the reflectivity of the mirror also increases the threshold current and is therefore less desirable. Decreasing the cavity length at first decreases the threshold current but then rapidly increases the threshold current.

Figure (3) shows the variation of amplitude of laser power at relaxation frequency to that at zero frequency with the relaxation frequency for

two different cases. The difference between values for two cases is too small except the deviation toward larger difference at the lower relaxation frequencies (ω_0), when we suppose that the effective lifetime (τ_{eff}) coincides the photon lifetime (τ_{ph}), which is in turn an ideal case. As the effective lifetime being longer, the photon inside laser cavity has much more chances to stimulate the laser active medium to produce much more photons, hence much more power. This can be achieved by maximizing the photon lifetime throughout two main parameters; the first is minimizing the losses inside cavity, and the second is optimizing both cavity length and front mirror reflectivity.

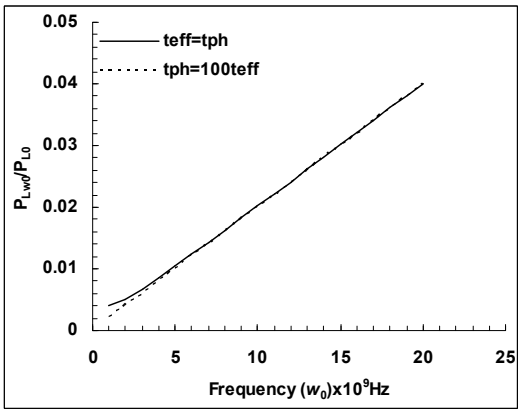

Fig. (3) Variation of amplitude of laser power at relaxation frequency to that at zero frequency with the relaxation frequency for two different cases: equal photon and effective lifetimes (continuous line) and effective lifetime shorter by two orders of magnitudes than the photon lifetime (dashed line)

Figure (4) shows the variation of threshold current density (J_{th}) with the number of quantum wells in the laser structure (m). According to Eq. (28) and Fig. (4), the threshold current density is a constant plus a component which is proportional to the number of quantum wells. Threshold current density increases fast as the number of quantum wells does within hundreds range, whilst it keeps increasing slowly as the number m keeps increasing through thousands. Due to structural reasons, there is a limit for the number of quantum wells inside laser structure as the latter can terminate over such limits. According to Eqs (18) and (26), we would work to increase the gain by increasing the carrier density but this procedure imposes much more wells (higher m), which increases the threshold current density required for the optimum performance of laser device. On the other side, decreasing carrier density imposes decreasing gain (g) as well as decreasing threshold current density as the number of quantum wells (m) will decrease too. Therefore, compensation in all parameters mentioned above should be taken into account to optimize the performance of the supposed laser design.

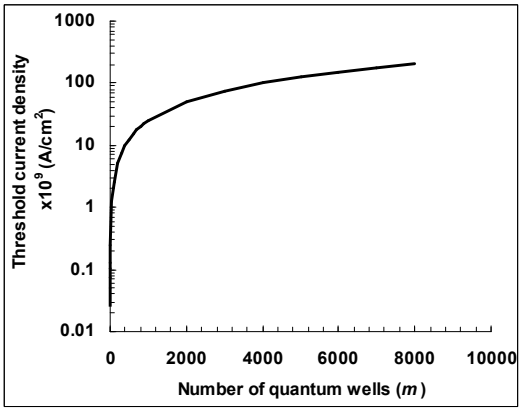

Fig. (4) Variation of threshold current density (J_{th}) with the number of quantum wells in the laser structure (m)

4. Conclusions

From the results of analytical treatments presented in this study, the optimum performance of multi-quantum wells lasers is determined by several physical and engineering considerations. These considerations can be reduced to some parameters those are controlled by earlier design steps. Both cavity length and front mirror reflectivity are controlled to determine the quantum efficiency of laser system, hence, the effective lifetime is controlled to maximize the laser power at the relaxation frequency. As well, the number of quantum wells in the laser structure is a parameter to control threshold current density.

References

[1] J. Mulet, M. Kroh and J. Mørk, *Opt. Express*, 14(3) (2006) 1119-1124.
[2] U. Koren et al., *Appl. Phys. Lett.*, 51 (1987) 1744-1746.
[3] A. Kasukawa, I. Imajo and T. Makino, *Electron. Lett.*, 25 (1989) 104-105.
[4] T.L. Koch et al., *Electron. Lett.*, 24 (1988) 1431-1432.
[5] N.J. Holonyak, R.M. Koblas and R.D. Dupuis, *IEEE J. Quantum Electron.*, QE-16(2) (1980) 170-185.
[6] J. Kaiser et al., *IEEE J. Selected Topics in Quantum Electronics*, 10(5) (2004) 968-973
[7] K.A. Williams et al., *IEEE Journal of Selected Topics in Quantum Electronics*, 5 (1999) 822-31.
[8] S. Sujecki et al., *IEE Proc. Optoelectronics*, 150(3) (2003) 246-252.

Optical Properties of Thermally-Annealed Tin-Doped Indium Oxide Thin Films

Azhar I. Hasan

School of Applied Sciences, University of Technology, Baghdad, Iraq

In this work, results of thermal annealing of tin-doped indium oxide thin films were presented. The effect of thermal annealing of the optical characteristics of such films was introduced. These characteristics include transmission, absorption coefficient, absorption depth, type of band gap and the dominant absorption processes. Thermal annealing may improve the diffusion of Sn dopants in the In_2O_3 structure and hence affect the optical properties of the resulted structure. The Sn-doped In_2O_3 thin films are widely used in the optoelectronics and integrated optics architecture.

Keywords: In_2O_3, Thermal evaporation, Annealing conditions, Optical properties
Received: 21 October 2008, **Revised**: 28 April 2009, **Accepted**: 10 May 2009

1. Introduction

Thin films made of metal oxides have some distinct characteristics such as good electrical conductivity, high optical transmission in the visible wavelengths region, good adhesion on crystalline and amorphous substrates, chemical stability and excellent photochemical properties. These characteristics are originated from the behavior of such materials as n-type semiconductors with wide energy bandgap. Examples of such films are indium oxide (In_2O_3) deposited on glass substrate and tin-doped indium oxide (Sn-doped In_2O_3). These films are widely used in solar conversion devices, photovoltaic devices and flat displays [1-3].

Too many recent and advanced applications impose using of In_2O_3 films with low electrical resistance and high transmission in the visible region. So, in order to optimize such properties, several parameters, such as films thickness, doping type and concentration, and deposition conditions, should be controlled. Accordingly, a figure of merit should be determined to introduce the quality of the transparent conducting oxides (TCOs) [4,5].

The electrical and optical properties of the semiconducting oxides, like In_2O_3, highly depend on the density of defects resulted from the external doping as well as their preparation and growth conditions [6]. Tin (Sn) is the much suitable materials to perform the external doping in indium oxide other than fluorine (F), chlorine (Cl) and antimony (Sb) [7]. It is important to control the concentration of tin dopants those replace In_2O_3 molecules in the lattice in order to obtain low-resistance films. When a tin atom replaces indium atom, it releases a free electron inside the lattice, hence, the electrical conductivity is increased. However, this atom will also act as a scattering center since it is neutral; hence, the electrical conductivity is decreased [8].

Indium oxide films can be prepared by several techniques, such as DC sputtering, RF sputtering, chemical vapor deposition (CVD), thermal evaporation and spray pyrolysis [9-13].

In this work, tin thin films were deposited on In_2O_3 layer then thermal annealing was performed to obtain Sn-doped In_2O_3 films and enhance their optical properties.

2. Experiment

High purity (99.999) indium oxide was used to deposit thin films on glass substrates using vacuum evaporation system (Balzer-80) at vacuum pressure of 10^{-6}torr. The deposited films were about 500nm in thickness, which was determined by the weighing method. The optical measurements were carried out on the prepared In_2O_3 films then thin films of tin were deposited over the In_2O_3 films with different thicknesses. The optimum results were found at 30nm Sn film. An electronically-controlled furnace was used for thermal annealing of the Sn/In_2O_3 structures. The transmission measurements were performed within the wavelength range of 300-90nm using GECIL GE-720 spectrophotometer.

3. Results and Discussion

Figure (1) shows the transmission spectrum of the prepared samples of Sn-doped In_2O_3 for three different cases (without thermal annealing, 600K annealing and 800K annealing). The transmittance is continuously increased with the incident wavelength. The transmission in this case is mainly determined by absorption

coefficient and thickness of the sample as tin atoms are not stimulated to diffuse inside the In_2O_3 structure. Therefore, the optical properties of the sample are fundamentally belonging to the under-layer material (In_2O_3) as the thickness of tin layer is too small to affect the transmission.

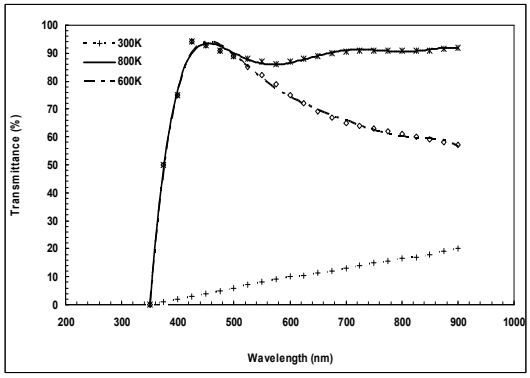

Fig. (1) Transmittance of the prepared samples in both cases (without annealing, at different annealing temperatures)

In case of thermal annealing at 600K, tin atoms are stimulated to diffuse inside In_2O_3 structure according to Fick's law [14]:

$$D = D_0 \exp(-\frac{E_a}{K_B T}) \quad (1)$$

where E_a is the activation energy of the dopants (tin atoms), D is the temperature-dependent diffusion coefficient and D_0 is the diffusion coefficient at 0K

As shown in Fig. (1), in cases of annealing at 600K and 800K, the transmittance is rapidly increased for wavelengths shorter than 450nm, where the transmittance is slightly decreased. The rapid increase is attributed to the effect of tin atoms diffusion and formation of a Sn-doped In_2O_3 layer. Indium oxide has too high sensitivity to doping as its optical and electrical properties are highly changed with the doping type and concentration.

The transmission spectrum at annealing temperature of 800K is clearly distinguished from that at 600K above 480nm as the latter (600K) is decreased to reach 57% at 900nm while the former (800K) is slightly decreased then slowly increased over 600nm to reach about 92% at 900nm.due to Fick's law, the diffusion coefficient of tin atoms inside indium oxide structure at 600K is smaller than that at 800K. Therefore, the electrical and optical characteristics may differ depending on the diffusion depth of dopants as well as their distribution profile inside the substrate (In_2O_3).

At the beginning, the Sn films did not affect the transmission of In_2O_3 because tin atoms were not yet stimulated by annealing to diffuse inside the In_2O_3 structure. After annealing of In_2O_3 films, the effect of tin atoms diffusion and formation of a Sn-doped In_2O_3 layer made In_2O_3 films to be high sensitive for doping.

Figure (2) represents the variation of absorption coefficient with incident photon energy. The absorption coefficient was determined from the following relation:

$$\alpha = -\frac{1}{t}\ln(T) \quad (2)$$

where t is the thickness of sample (in cm) and T is the transmittance (%)

The different behavior of the function with incident photon energy is attributed to the diffusion of tin atoms those act as dopants inside In_2O_3 structure [15]. As shown, there several regions can be distinguished. In the first region (>828nm), the absorption coefficient is increased with photon energy to its peak at 1.5eV corresponding to wavelength of 828nm. In this region, the absorption by impurities is the dominant absorption process as the incident photon energy is higher than impurity ionization energy (0.025eV) but lower than the energy bandgap of the semiconductor. So, the absorption coefficient is given by:

$$\alpha_{imp} = N_T.\sigma \quad (3)$$

where N_T is the concentration of unionized impurities and σ is the absorption cross section, which is dependent of temperature, concentration of impurities and their ionization energy

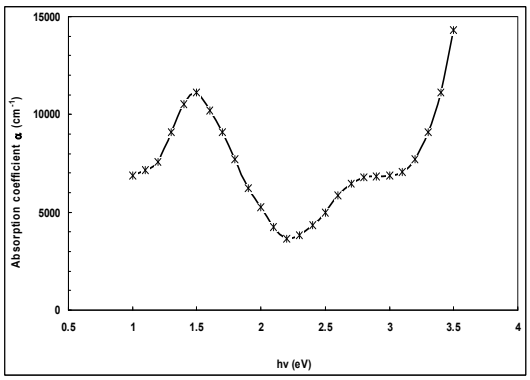

Fig. (2) Variation of absorption coefficient with incident photon energy for the sample annealed at 800K

In the second region (566-828) nm, the absorption coefficient is decreased with increasing photon energy because the absorption is achieved by the substrate material (In_2O_3) and the dopants have no more effect on absorption process since the incident photon passes the region through which tin atoms diffuse to reach indium oxide layer. This behavior is a general feature of semiconductors with varying incident photon energy below the cutoff wavelength. The absorption coefficient has a minimum at 566nm.

In the third region (<566nm), the absorption coefficient is increased with incident photon energy as the fundamental absorption processes

are the dominant since the incident photon energy is higher than or equal to the direct energy bandgap of the semiconductor (~2.6eV). This increase is continued within the ultraviolet (UV) region of wavelengths and a small region of approximately constant absorption coefficient appears within 415-434nm.

The behavior in the third region may support the assumption that direct and indirect transitions occur at these values of incident photon energy with a probability depending on selection rules those governing inter-level transitions between valence and conduction bands as well as the effect of tin atoms on the type of bandgap in the semiconductor [16].

In order to determine either the direct or the indirect transitions are the dominant, the adsorption depth was sketched with incident photon energy. The value of adsorption depth for the fundamental direct absorption processes is ranging within 100-1000nm while it is expected to be 10m, for the indirect processes. As shown in Fig. (3), the fundamental indirect absorption processes are the dominant with a small occurrence probability for the direct ones. Thermal annealing of the prepared samples lead to increase the adsorption depth to its maximum (5um), after which it rapidly decreases at high energy regions (short wavelengths).

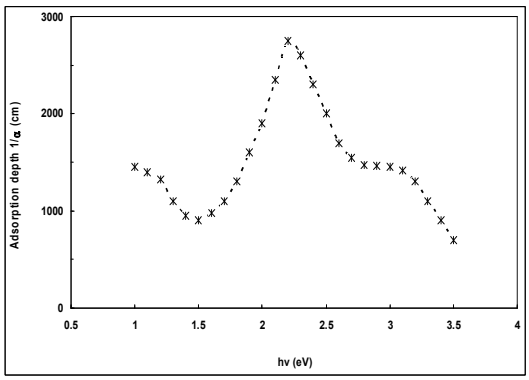

Fig. (3) Variation of adsorption coefficient with incident photon energy for the sample annealed at 800K

Figure (4) shows the relation between the function $(\alpha hv)^{1/2}$ and the incident photon energy (hv) and the linear function confirms that the fundamental indirect absorption processes are the dominant, i.e., the semiconductor has an indirect energy bandgap. Such semiconductors are widely used for manufacturing semiconductor lasers, narrow-response quantum detectors, multi-quantum wells structures and their devices.

However, there is a probability for the forbidden fundamental direct absorption processes to occur since indium oxide has a direct bandgap of about 3.75eV and an indirect bandgap of about 2.6eV. Therefore, controlling the doping of such materials make possible to control their optical properties to serve some required applications. Accordingly, the doped indium oxide is currently one of the most important materials used for building integrated optics those moving dramatically fast to replace the integrated circuits together with the enormous developments of optical communications and their wide applications [17].

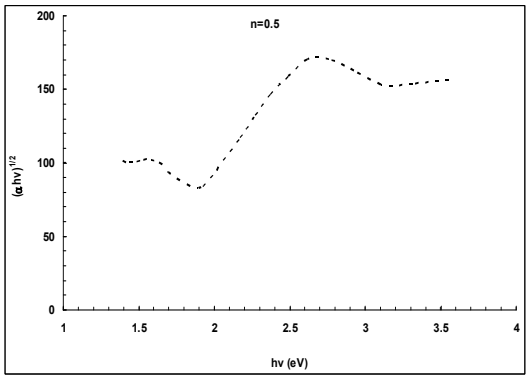

Fig. (4) Variation of $(\alpha hv)^{1/2}$ with incident photon energy for the sample annealed at 800K

4. Conclusion

Due to the results obtained from this work, thermal annealing lead to change the optical properties of tin-doped indium oxide samples as their transmission in the visible and near-infrared regions was increased. Accordingly, the absorption characteristics in these regions was changed too leading to obtain an extrinsic semiconductor in which the fundamental indirect absorption processes dominate with lesser probability for the direct processes to occur. As a consequence of annealing, this material became a candidate to serve different applications of optoelectronics in several spectral regions. As well, the semiconductor having different types of absorption processes is very important in the architecture of advanced optical communications systems.

References

[1] S.M. Sze, **"Semiconductor Devices: Physics and Techniques"**, John-Wiley & Sons (NY), 1981.

[2] G. Haacke, *J. Appl. Phys.* Vol.47, 1976, 4086-4089.

[3] I. Hamberg and C.G. Granquist, *Appl. Phys. Lett.* Vol. 40, 1982, 362-367.

[4] B.E. Yoldas and P.W.Patrlow, *Thin Solid Films*, Vol. 129, 1985, 1-14.

[5] S. Ohno et al., *Sci. and Technol. of Adv. Mater.*, 7 (2006) 56-61.

[6] M. Just, N. Maintzer and I. Blech, *Thin Solid Films*, Vol. 48, 1978, L19-L20.

[7] W.W. Molzen, *J. Vac. Sci. Technol.*, Vol. 12, 1975, 99-105.

[8] J.C.C. Fan and F.J. Bechuer, *J. Electrochem. Soc.*, Vol. 112, 1975, 1718-1723.
[9] Y. Ohhata, F. Shinoki and S. Yoshida, *Thin Solid Films*, Vol. 59, 1979, 255-261.
[10] K. Pommier, C. Gril and J. Marucchi, *Thin Solid Films*, Vol.77, 1981, 91-98.
[11] J. Smith, A. Aronson, D. Chen and W. Class, *Thin Solid Films*, Vol. 72, 1980, 469-474.
[12] A. Ambrosini, A. Durate, K. Poeppelmeier, M. Lane, C. Kannewurf and T. Mason, *J. Solid State Chem.*, Vol. 153, 2000, 41-47.
[13] P. Psuja, D. Hreniak and W. Strek, "The influence of sintering temperature and Sn^{4+} concentration on electrical and optical properties of ITO nanocrystallites", 2nd National Conf. on Nanotechnology, *J. of Phys.: Conf. Series*, 146 (2009) 012.
[14] J.F. Shackelford **"Introduction to Material Science For Engineers"**, 5th ed., Prentice-Hall, Inc., New York (2000) 167.
[15] Y. Zhong et al., *J. Mater. Res.*, 23(9) (2008) 2500-2505.
[16] D. Kalhor et al., *World Appl. Sci. J.*, 6(1) (2009) 83-87.
[17] S.H. Mohamed et al., *Acta Physica Polonica A*, 115(3) (2009) 704-708.

Selma M.H. Al-Jawad
Zahra'a S. Ahmed
Wessal A. Taha

School of Applied Sciences, University of Technology, Baghdad, Iraq

Optical Properties of Annealed Cadmium Sulfide Thin Films Prepared by Chemical Bath Deposition

CdS thin films were prepared by the chemical bath deposition technique. Annealing in air at different temperatures (300, 350, 400, 450, and 500)°C at constant time of 30min, also for different times (15, 30, 45, 60, and 90) min at constant temperature (300°C) is achieved. The CdS films showed, on average, 20% reflectance. The transmittance ranged between 80–92% for the films annealed at 60 and 45 min. On average, the refractive index of the CdS is 1.2 and the band gap is 2.4eV, the wide band gap semiconductor has a wide range of applications in areas including photocells and other photoconductive devices.

Keywords: CdS, Chemical bath deposition, Annealing conditions, Optical properties
Received: 31 March 2009, **Revised**: 30 April 2009, **Accepted**: 11 May 2009

1. Introduction

There are many deposition techniques used to deposit thin film semiconductors, such as (evaporation, sputtering, spray pyrolysis, chemical bath deposition). The preparation of thin films by a chemical deposition process is advantageous because of its simplicity, ease and economic ability and the adjusting of the semiconductor properties by band-gap variation, doping, control over stiochiometry, etc., can be accomplished with greater accuracy [1].

Cadmium sulfide (CdS), an important [2] compound semiconductor, has a typical wide band gap of 2.4eV at room temperature [3]. The CdS compound semiconductors exhibit excellent electrical, chemical and optical properties which make them one of the promising candidates in the field of photovoltaic energy conversion. Direct band gap thin film cadmium sulfide has been the subject of intensive research because of its intermediate band gap, high absorption coefficient, reasonable conversion efficiency and stability [4]. Also it is used in light amplifiers, radiation detectors, thin film transistor and diodes [1], piezoelectric transducers, laser

Most CBD films reported are fairly transparent to very transparent, typically between 60 and 90% transparent in the subband gap region [7,8]. Annealing of the films increases [8] or decrease [9] the optical transmission, according to annealing condition and deposited film component. The absorption edge shifts towards lower energy region and decrease in the band gap [5,8,9], this is due to the interference effect in the compressed multilayered structure formation of CdS after annealing [8] while Grecu et al. attributed the decreasing of band gap for annealed films at (500°C) to a possible contamination with cadmium hydroxide as source of (CdO) [2]. George et al. related the decrease in the band gap in the heated films to the grain size growth and composition change taking place in the films [10].

The aim of this paper is study the optical properties of annealed CdS films prepared by CBD method. The effect of annealing at different temperature and time is reported.

2. Experimental Work

Substrate used for deposition CdS is borosilicate glass slides, which were first cleaned in distilled water in order to remove the impurities and residuals from their surfaces, followed by rinsing in chromic acid (for one day), to introduce functional groups called nucleation and/or epitaxial centers, which formed the basis for the thin films growth [11]. Then the samples were washed repeatedly in deionized water, and finally put in ultrasonic agitation with distilled water for 15 min then dried.

Cadmium sulfide films were prepared from cadmium sulfate and thiourea by chemical bath deposition in alkaline solution. Films were deposited on glass slides by, 30ml of 0.1M ($3CdSO_4.8H_2O$), 30ml NH_3 solution and distilled water were mixed slowly at room temperature with continuous stirring. Substrates were then immersed in a beaker containing the reaction mixture. The beaker was placed in a water bath at temperature (80±2°C). The solution was stirred with a magnetic stirrer type (MSH 300). Then, it was heated with continuous stirring to the required temperature of deposition, 30ml of 0.2M thiourea solution was then added with

continuous stirring, and the pH measured with pH meter (type BIBBY). Substrates were then taken out after a suitable time; they were washed with distilled water and ultrasonic agitation to remove the porous cadmium sulfide over layer, then dried. All the samples were annealed in a furnace at different temperatures (300,350, 400, 450, and 500)°C for 30 min and different time (15, 30, 45, 60, 90) min at 300°C.

3. Measurements

A Cecile CE 7200 Spectrophotometer supplied by Aquarius Company was used to record the optical transmission and absorbance for CdS/glass thin films in the range (375–900nm). The data from transmission spectrum can be used in the calculation of the absorption coefficient (α) for CdS films, according to the following equation [13]:

$$\alpha = \frac{1}{d}\ln\frac{1}{T} \qquad (1)$$

where d is the thickness of thin film and T is the transmission

In the direct band gap structure or direct transition semiconductors (present case), the absorption coefficient and optical band gap (E_g) are related by [14]:

$$\alpha = (h\upsilon - Eg)^{1/2} \qquad (2)$$

where h is Plank's constant and ν is the frequency of the incident photon

The reflectance at normal incidence can be expressed in terms of the optical constants n and K as follows [15]:

$$R = \frac{(n-1)^2 + K^2}{(n+1)^2 + K^2} \qquad (3)$$

where n is the refractive index

In the range of frequencies in which the films are weakly absorbing $K^2 << (n\text{-}1)^2$, the following can be expressed [15]:

$$R = \frac{(n-1)^2}{(n+1)^2} \quad \text{or} \quad n = \frac{(1+R^{1/2})}{(1-R^{1/2})} \qquad (4)$$

Film thickness is measured by optical interferometer method. The method is based on interference of the light beam reflection from thin film surface and substrate bottom. He-Ne laser (632nm) was used for this purpose and the thickness is determined using the formula:

$$d = \frac{\Delta x}{x}.\frac{\lambda}{2} \qquad (5)$$

where x is fringe width, Δx is the distance between two fringes and λ is the wavelength of laser light

4. Results and Discussions

The optical transmission spectra depend on the chemical and crystal structures of the films, and also on the film thickness and on films surface morphology. We have found that the films have high transmission at long wavelengths (70-80%), which decreases to (10%) at short wavelengths.

Annealing of the as-deposited films decreases the optical transmittance and the absorption edge shifts towards lower energy region and becomes much sharper as shown in Fig. (1).

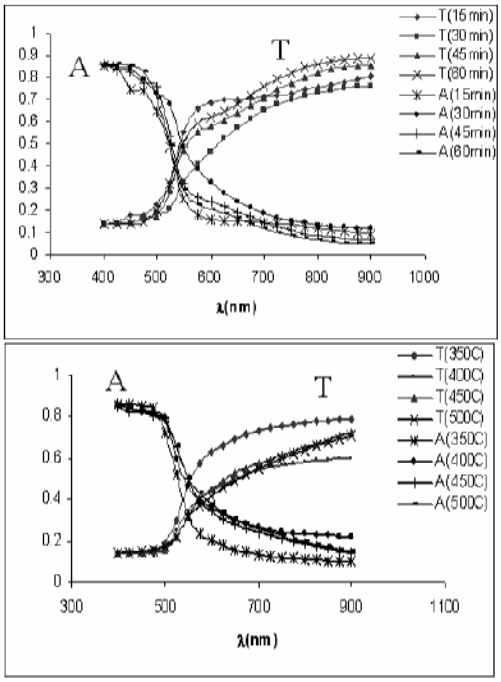

Fig. (1) Optical transmission spectra and absorption of CdS films at different annealing times (above) and different annealing temperatures (below)

The change of annealing conditions has a higher influence on the specular reflectance of CdS films, as shown in Fig. (2).

In general, the energy gap values depends on the films crystal structure, the arrangement and distribution of atoms in the crystal lattice, also it is affected by crystal regularity. The energy gap (E_g) value is calculated by extrapolation of the straight line of the plot of $(\alpha h\nu)^2$ versus photon energy for different annealing conditions as shown in Fig. (3). The linear dependence of $(\alpha h\nu)^2$ with $h\nu$ indicates that the films have direct band gap. Figure (3) shows the effect of annealing conditions on band gap, where the band gap value is estimated by extrapolation of the straight line of the plot of $(\alpha h\nu)^2$ versus photon energy. The annealed samples show a relative decrease in band gap with both annealing temperature and time. These results are consistent with the previously published results [10] in which the decrease in the band gap of the annealed samples was attributed to the grain size growth and composition changes taking place in the samples by CdO. Conversely, Archbold [16] attributed his results to either the phase transition from the cubic-to-hexagonal, or a reduction in strain within the film structure.

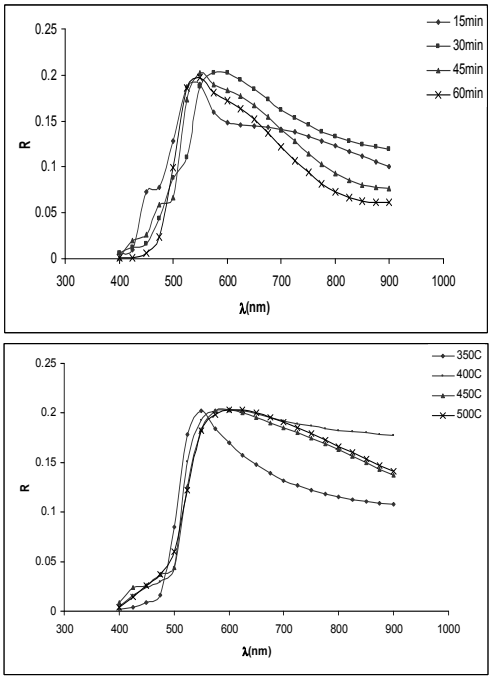

Fig. (2) Optical reflection spectra of CdS films at different annealing times (above) and different annealing temperatures (below)

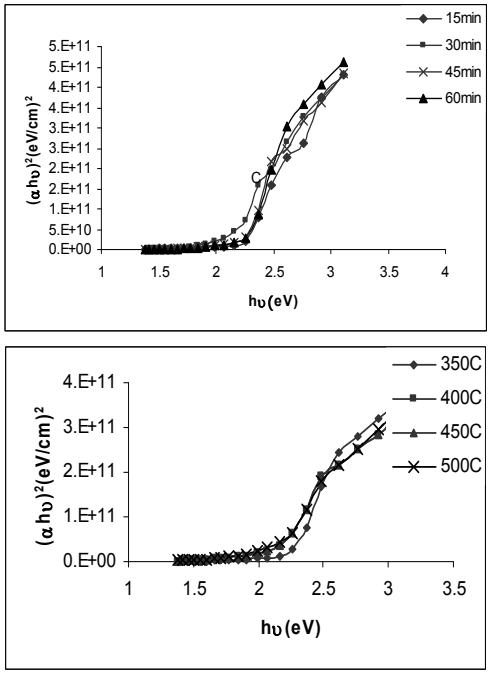

Fig. (3) Plot of $(\alpha h\nu)^2$ versus $(h\nu)$ at different annealing times (above) and different annealing temperatures (below)

Variation of the extinction coefficient with wavelength shown in Fig. (5). The linear relationship indicates sharp increase in the absorption with increasing wavelength. This conforms to the relation:

$$K = \frac{\alpha\lambda}{4\pi} \qquad (6)$$

where K is the extinction coefficient and α is the absorption coefficient

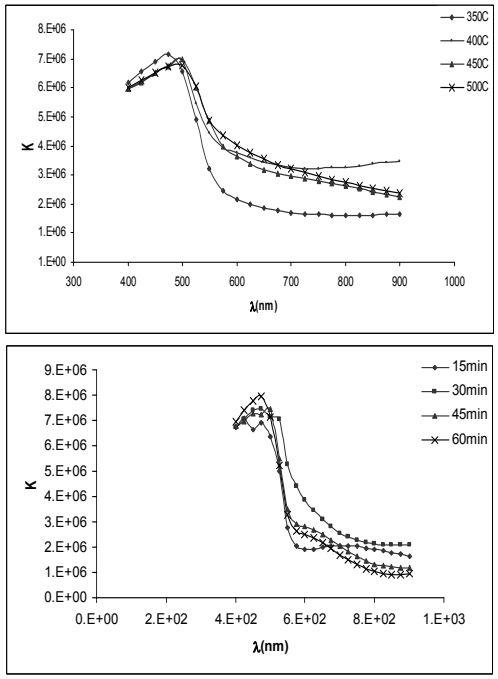

Fig. (5) Variation of extinction coefficient (K) with wavelength (λ) at different annealing times (above) and different annealing temperatures (below)

The refractive index (n) is the range of frequencies in which films are weakly absorbing. Figure (6) shows the variation of refractive index of CdS with wavelength. Refractive index of CdS is nearly equal to 1.2, which means that electromagnetic radiation is 1.2 times slower in the films than in the free space.

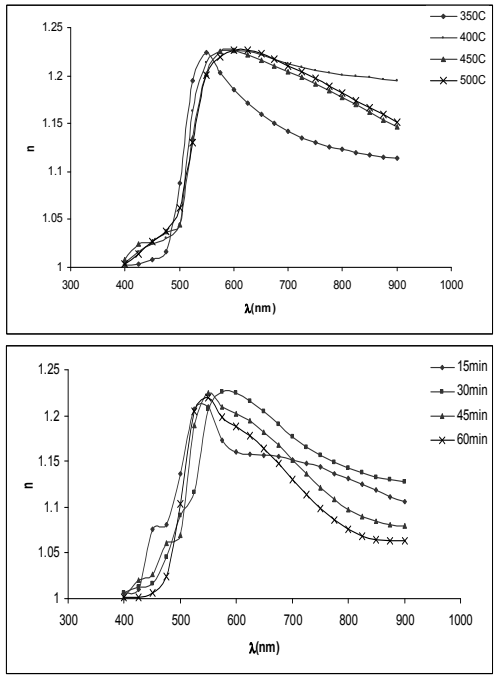

Fig. (6) Refractive index (n) as a function of wavelength (λ) at different annealing times (above) and different annealing temperatures (below)

The values of dielectric constant (ε_r) and optical conductivity (σ) have increased from the minus values in low energy regions to peak values at 2.4eV in the higher energy region and then decreased to low values in the same regions. The dielectric constant (ε_r) and optical conductivity (σ) are shown in Fig. (7) and (8).

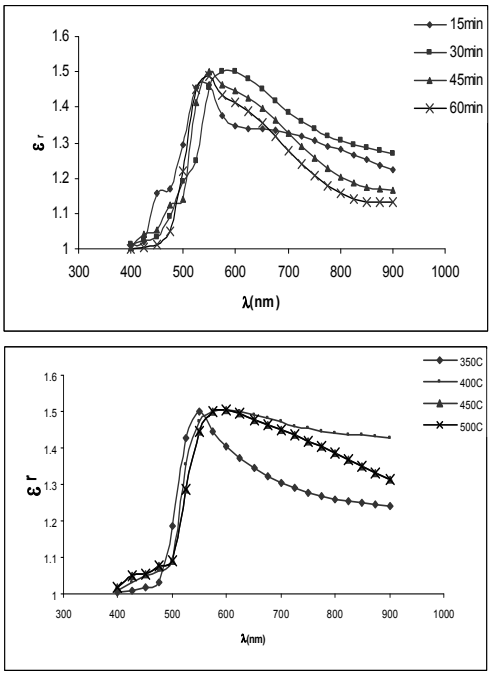

Fig. (7) dielectric constant (ε_r) as a function of wavelength (λ)at different annealing times (above) and different annealing temperatures (below)

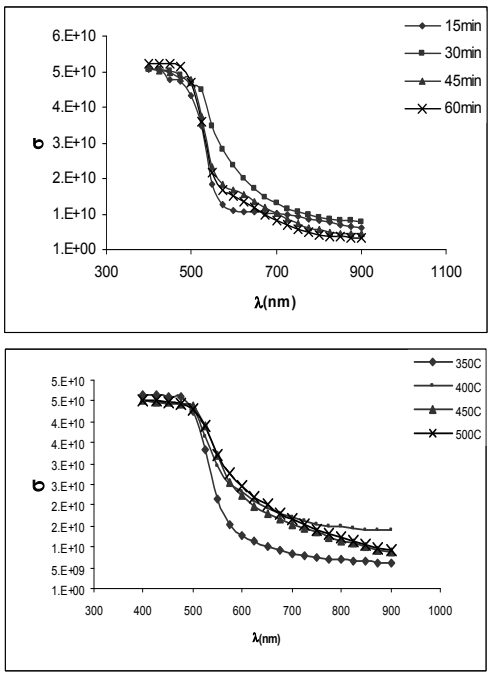

Fig. (8) Optical conductivity (σ) as a function of wavelength (λ) at different annealing times (above) and different annealing temperatures (below)

5. Conclusion

CdS thin films were successfully deposited in an alkaline medium using the chemical bath technique. The disparity between the properties of the films as grown and those annealed at higher temperature is a result of grain size growth and composition changes taking place in the samples by CdO. On average, CdS films show a reflectance in the range (5-20%) in the near infra-red region. They also have refractive index of 1.2 and band gap of 2.4eV.

References

[1] P.K. Nair and M.T.S. Nair, *Solar Cells*, 22 (1987) 103-112.
[2] K. Othmer, "Encyclopedia of chemical technology", Second Edition, Vol. 3, John-Wiley & Sons, Inc., (1964).
[3] A. Ashour, *Turk J. Phys.*, 27 (2003) 551-558.
[4] L.P. Deshmukh, A.B. Palwe and V.S. Sawant, Solar Energy Materials, 20, 1990, 341-348.
[5] R. Grecu et al., J. Optoelectro. Adv. Mater., 6(1) (2004) 127-132.
[6] S.N. Sahu and S. Chandra, *Solar Cells*, 22 (1987) 163-173.
[7] M.B.O. Lopez et al., *Thin Solid Films*, 457 (2004) 278-284.
[8] G. Sasikala, P. Thilakan and C. Subramanian, *Solar Energy Materials & Solar Cells*, 62 (2000) 275–293.
[9] W.J. Danaher, L.E. Lyons, and G.C. Morris, *Solar Energy Materials*, 12 (1985) 137-148.
[10] P.J. George et al., *Appl. Phys. Lett.*, 66(26) (1995) 3624-3626.
[11] G. Hodes et al., *Phys. Rev. B*, 36(8) (1987) 4215-4221.
[12] D.W. Cunningham et al., 29 IEEE PV Specialist Conf., New Orleans, Louisiana, May 20-24 (2002).
[13] K.K. Nanda et al., *Thin Solid Films*, 322 (1998) 21-27.
[14] E. Pentia et al., 5th General Conf. of the Balkan Physical Union, August 25-29 (2003), Vrnjacka Banja, Serbia and Montenegro, 799-802.
[15] M.J. Seong et al., Appl. Phys. Lett., 82(2) (2003) 185-187.
[16] M.D. Archbold et al., 31st IEEE Photovoltaic Specialists Conf., Coronado Springs Resort Lake Buena Vista, FL, January 3-7 (2005).

MNC 2009

22nd International Microprocesses and Nanotechnology Conference November 16-19, 2009

Conference Site:
Sheraton Sapporo Hotel, Sapporo, Japan

MNC 2009 SCOPE and SYMPOSIUM
1-1: DUV, EUV Lithography and Metrology
1-2: Electron- and Ion-Beam Lithography
1-3: Resist Materials and Processing
2-1: Nanodevices
2-2: Nanofabrication
2-3: Nanomaterials
2-4: Nano-Tool
3: Nanoimprint, Nanoprint and Rising Lithography
4: Bio MEMS, Lab on a Chip
5: Microsystem Technology and MEMS
Symposium A. Computational Lithography
Symosium B. Graphene: Growth & Characterization
Sponsored by
The Japan Applied Physics Physics

Committee Chairs:
Organizing Committee Chair:
S. Shoji (Waseda Univ.)
Steering Committee Chair:
T. Itani (Selete)
Program Committee Chari:
T. Meguro (Tokyo Univ. of Sci.)

Sponsored by
The Japan Society of Applied Physics

Cooperation
Association of Super-Advanced Electronics Technologies
The Institute of Electrical Engineers of Japan
The Institute of Electronics, Information and Communication Engineers
The Japan Society for Precision Engineering
The Japanese Society for Synchrotron Radiation Research
The Japanese Society of Electron Microscopy
The Surface Science Society of Japan
The Vacuum Society of Japan

MNC 2009 SCOPE and SYMPOSIUM

1-1:DUV, EUV Lithography and Metrology
This session focuses on DUV, EUV, Immersion Lithography, and Computational Lithography including OPC, SMO, DFM. In addition, Metrology such as SEM and Scatterometry is included.

1-2:Electron- and Ion-Beam Lithography
Electron and ion beam technologies such as lithography, metrology, inspection and repair tools. Other related technologies using charged particle beams are also welcome.

1-3:Resist Materials and Processing
Resist materials(EUV, immersion, double patterning, DUV, EB, X-ray, multilayer, inorganic, molecular glass etc.), antireflective coatings, polyimide, adhesive, and other materials related to lithography. resist processes (PEB, development, rinse, resist removal, etching etc.)characterization, line edge roughness, trade-off problem, outgassing, modeling and simulation of resist process (exposure, acid diffusion, development etc.). materials and processes for the production of flat-panel display, photonics devices, and electronics packaging.

2-1:Nanodevices
Nanodevices and related technologies targeting more Moore, more than Moore and beyond CMOS; next-generation Si and compound semi conductor-based FETs, graphene FETs, 1D FETs such as nanowire FETs and carbon nanotube FETs, quantum dot devices, and all other nanodevices utilizing nanostructures and nanomaterials such as inorganics, organics, and molecules. Novel-concept devices utilizing nanostructures and nanophysics are also welcome.

2-2:Nanofabrication
Fabrication of nanostructures. Fabrication techniques such as scanning probe techniques, self-organizing techniques, etc. Physics and chemistry in nanofabrication processes. Etching, deposition, and related subsurface processing using photon, electron- and ion-beams, plasma, and thermal energy. Emerging technologies are also welcome.

2-3:Nanomaterials
Theory, properties, characterization and application of nanomaterials such as quantum dots, nano-particles, nanowires, carbon nanotubes, fullerenes, organic, molecular, and biomaterials. Materials prepared by self-organized or bottom-up approach are also included.

2-4:Nano-Tool
Nano-electromechanical system (NEMS), Nano-mechanics, Nanometrology, Metrology and repair for nanosystem, Novel observation and fabrication methods based on microscopic techniques, such as scanning probe microscopy (SPM), scanning electron microscopy (SEM) and focused ion beam (FIB).

3:Nanoimprint, Nanoprint and Rising Lithography
This session focuses nanoimprint system, process, material, applications and related inspection and metrology. Other novel nano-patterning technologies are also included. This session focuses nanoimprint system, process, material,applications and related inspection and metrology. Other novel patterning technologies are also included.

4:Bio MEMS, Lab on a Chip
Micro/nano electromechanical devices (M/NEMS) are now widely applied to biochemical, medical and environmental fields and a new research field called μ-TAS or Lab. on a Chip is expanding. Fusion of microelectronic devices with materials and methods in the

biomedical fields is expected to open up new scientific and business areas. Papers are solicited in the following areas (but not limited): (1) MEMS/NEMS devices for biomedical fields, (2) μ-TAS and Lab on a chip, (3) Bio-chips for DNA, proteins and cells, (4) Fabrication technologies.

5:Microsystem Technology and MEMS
Fabrication techniques, design, mechanical characterization of three dimensional microstructures, and their applications to micromechanical systems, which include microwave and photonics devices, vacuum microelectronics, novel sensors and actuators, etc.

Symposium A. Computational Lithography
Symosium B. Graphene: growth & characterization

PLENARY SPEAKERS
S. Wurm (SEMATECH) A. Neureuter (Univ. of CA)
INVITED SPEAKERS
DUV, EUV Lithography and Metrology Session **T. Uchiyama (NEC Electronics)** Electron and Ion Beam Lithography Session **H. Loeschner (IMS Nanofabrication)** Resist Materials and Processing Session **M. Shirai (Osaka Pref. Univ.)** Nanodevice Session **Y.-M. Lin (IBM)** Nanofabrication Session **T. Fukui (Hokkaido Univ.)** Nanomaterials Session **Y. Einaga (Keio Univ.) I. Suemune (Hokkaido Univ.)** Nano-Tool Session **T. Funatsu (Univ. of Tokyo)** Nanoimprint, Nanoprint and Rising Lithography Session **H. Schift (Paul Scherrer Inst.) Q. Xia (HP)** Bio MEMS, Lab on a Chip Session Microsystem Technology and MEMS Session Symposium A. Computational Lithography **K. Lai (IBM) A. Erdmann (Fraunhofer) T. Matsuyama (Nikon) T. Takigawa (Brion Technologies) L. Pang (Luminescent Technologies) M. D. Smith (KLA-Tencor) W. Demmerle (Synopsys)**

Organizing Committee Members
Chair
S. Shoji (Waseda Univ.)
Vice Chair
T. Asano (Kyushu Univ.)
T. Fukui (Hokkaido Univ.)
Members
H. Arimoto (Fujitsu), R. Ebinuma (Canon), K. Fujii (NEC Electronics), N. Fukushima (Toshiba), K. Hane (Tohoku Univ.), N. Hayashi (Dai Nippon Printing), Y. Horiike (NIMS), T. Horiuchi (Tokyo Denki Univ.), K. Ishibashi (Riken), A. Ishihama (Sharp), S. Ishihara (Univ. of Tokyo), S. Kadomura (Sony), M. Kameyama (Nikon), M. Komuro (NEDO), S. Matsui (Univ. of Hyogo), I. Mori (Selete), Y. Ochiai (Toyo Gosei), S. Okazaki (Hitachi), S. Sato (Fujitsu Labs.), S. Tagawa (Osaka Univ.), Y. Todokoro (Nara Inst. Sci. & Technol.), H. Yamaguchi (NTT), N. Yoshioka (Renesas Technol.), S. Zaima (Nagoya Univ.)

Advisory Members
H. Ahmed (Cambridge Univ.), Y. Aoyagi (Ritsumeikan Univ.), S. Brueck (Univ. of New Mexico), C.Y. Chang (Natl. Nano Device Lab.), F. Fortagne (Leica Microsystem), K. Gamo (Osaka Univ.), E. Gogolides (IMEL, NCSR), C. Hanson (SPAWAR System), L.R. Harriott (Univ. of Virginia), O. Joubert (CRS-LTM), D. Kern (Univ. of Tubingen), H.W.P. Koops (NaWoTec GmbH), J. Melngailis (Univ. of Meryland), S.-K. Min (Kyung Hee Univ.), A.R. Neureuther (UC Berkeley), R.F.W. Pease (Stanford Univ.), C. Pfeiffer (Consultant), I. Raptis (IMEL, NCSR), R. Shimizu (IIAS), C. Shih (ERSO/ITRI), H.I. Smith (MIT), T. Sugano (Univ. of Tokyo), M. Takai (Osaka Univ.), S. Tedesco (Leti), T. Tsurushima (Kyushu Univ.), M. Wang (China Academic Sci.), J. Wiesner (Nikon Precision), N. Yokoyama (Fujitsu Labs.)

Steering Committee Members
Chair
T. Itani (Selete)
Vice Chair
Y. Miyamoto (Tokyo Inst. of Technol.)
Program
T. Meguro (Tokyo Univ. of Sci.)
Secretary
K. Nakano (NEC)
Y. Ono (NTT)
Treasure
Y. Ono (NTT)
S. Aoyama (Renesas)
Seminar
S. Kasai (Hokkaido Univ.)
F. Nihey (NEC)
Public Information
S. Akita (Osaka Pref. Univ.)
K. Tohmezuka (Tokyo Electron)
Publicity
H. Yamashita (HOYA)
T. Kozawa (Osaka Univ.)
Technical Exhibition
N. Sakai (Toyo Gosei)
N. Taneichi (Tokyo Ohka)
Place
S. Hara (Hokkaido Univ.)
M. Takeyama (Kitami Inst. of Technol.)
Overseas
J.H. Ahn (Hanyang Univ.)
A. Chen (ASML)
O.H. Kim (POSTEC)
C.K. Sung (National Tsing Hua Univ.)

Abstract Deadline: June 30 2009.

Late News Paper Deadline (2nd Abstract Deadline): September 15, 2009

Technical Seminar in Japanese is sponsored by Hokkaido Univ.

CONTACT US:
Secretariat for 22nd International Microprocesses and Nanotechnology Conference (MNC 2009)
c/o Secretaryart Corporation
TEL:+81-3-5367-1735
FAX:+81-3-5367-1736
Email: secretariat@imnc.jp

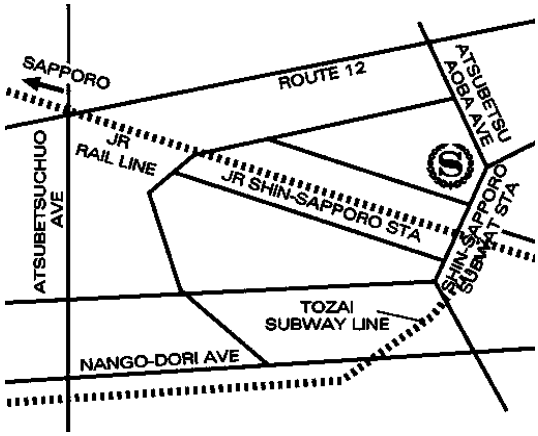

THE IRAQI JOURNAL OF APPLIED PHYSICS LETTERS
EDITORIAL BOARD

IJAPLett

COPYRIGHT RELEASE

Iraqi Journal of Applied Physics Letters (IJAPLett)

We, the undersigned, the author/authors of the article titled

……

……

……

……

that is presented to the Iraqi Journal of Applied Physics Letters (IJAPLett) for publication, declare that we have neither taken part or full text from any published work by others, nor presented or published it elsewhere in any other journal. We also declare transferring copyrights and conduct of this article to the Iraqi Journal of Applied Physics Letters (IJAPLett) after accepting it for publication.

The authors will keep the following rights:

1. **Possession of the article such as patent rights.**
2. **Free of charge use of the article or part of it in any future work by the authors such as books and lecture notes without referring to the IJAPLett.**
3. **Republishing the article for any personal purposes of the authors after taking journal permission.**

To be signed by all authors:

Signature:……..date: ……..
Printed name: ……..
Signature:……..date: ……..
Printed name: ……..
Signature:……..date: ……..
Printed name: ……..
Correspondence address:……..
……
……..
……
Telephone:……Fax:……email: ……..

Note: Please, complete and sign this form and mail it to the below address with your manuscript

The Iraqi Journal of Applied Physics Letters,
P. O. Box 55259, Baghdad 12001, IRAQ

Website: www.ijap.org, Email: ijaplett@ijap.org, ijaplett.editor@hotmail.com, Tel.: +964-7901274190

CONTENTS

VOL. 2 , NO. 2 , APRIL-JUNE 2009

  PRINTED IN IRAQ